

# Fermi polaron-polaritons in charge-tunable atomically thin semiconductors

Meinrad Sidler, Patrick Back, Ovidiu Cotlet, Ajit Srivastava<sup>†</sup>,

Thomas Fink, Martin Kroner, Eugene Demler\*, and Atac Imamoglu  
*Institute of Quantum Electronics, ETH Zürich, CH-8093 Zürich, Switzerland.*

<sup>†</sup>*Physics Department, Emory University, Atlanta, Georgia 22138, USA and*

*\*Physics Department, Harvard University, Cambridge, Massachusetts 02138, USA*

(Dated: March 31, 2016)

The dynamics of a mobile quantum impurity in a degenerate Fermi system is a fundamental problem in many-body physics. The interest in this field has been renewed due to recent ground-breaking experiments with ultra-cold Fermi gases [1–5]. Optical creation of an exciton or a polariton in a two-dimensional electron system embedded in a microcavity constitutes a new frontier for this field due to an interplay between cavity-coupling favoring ultra-low mass polariton formation [6] and exciton-electron interactions leading to polaron or trion formation [7, 8]. Here, we present cavity spectroscopy of gate-tunable monolayer MoSe<sub>2</sub> [9] exhibiting strongly bound trion and polaron resonances, as well as non-perturbative coupling to a single microcavity mode [10, 11]. As the electron density is increased, the oscillator strength determined from the polariton splitting is gradually transferred from the higher-energy repulsive-exciton-polaron resonance to the lower-energy attractive-polaron manifold. Simultaneous observation of polariton formation in both attractive and repulsive branches indicate a new regime of polaron physics where the polariton impurity mass is much smaller than that of the electrons. Our findings shed new light on optical response of semiconductors in the presence of free carriers by identifying the Fermi polaron nature of excitonic resonances and constitute a first step in investigation of a new class of degenerate Bose-Fermi mixtures [12, 13].

Transition metal dichalcogenide (TMD) monolayers represent a new class of two dimensional (2D) semiconductors exhibiting features such as strong Coulomb interactions [14], locking of spin and valley degrees of freedom due to large spin-orbit coupling [9] and finite electron/exciton Berry curvature with novel transport and optical signatures [15, 16]. Unlike quantum wells or two-dimensional electron systems (2DES) in III-V semiconductors, TMD monolayers exhibit an ultra-large exciton binding energy  $E_{exc}$  of order 0.5 eV [14] and strong trion peaks in photoluminescence (PL) that are red-shifted from the exciton line by  $E_T \sim 30$  meV [9, 17]. These features provide a unique opportunity to investigate many-body physics associated with trion [18] formation as well as coupling of excitons to a 2DES [19] and to cavity photons [20, 21], provided that the experimental set-up allows for varying the electron density  $n_e$  and light matter coupling strength  $g_c$ .

Here, we carry out an investigation of Fermi polarons [1] in a charge-tunable MoSe<sub>2</sub> monolayer embedded in an open microcavity structure (Fig. 1a-b). Since  $E_{exc}$  is much larger than all other relevant energy scales, such as the normal mode splitting ( $2g_c$ ),  $E_T$  and the Fermi energy ( $E_F$ ), an optically generated exciton in a TMD monolayer can be considered as a robust mobile bosonic impurity embedded in a fermionic reservoir (Fig. 1c). The Hamiltonian describing the system is

$$H = \omega_c c_0^\dagger c_0 + \sum_k \omega_X(k) x_k^\dagger x_k + g_c (c_0^\dagger x_0 + h.c.) + \sum_k \epsilon_k e_k^\dagger e_k + \sum_{k,k',q} V_q (x_{k+q}^\dagger e_{k'-q}^\dagger e_{k'} x_k + h.c.), \quad (1)$$

where the first line describes the coupling of 2D excitons, described by the exciton annihilation operator  $x_k$  and dispersion  $\omega_X(k) = -E_{exc} + k^2/2m_{exc}$ , to a zero-dimensional (0D) cavity mode  $c_0$  whose resonance frequency  $\omega_c$  can be tuned by applying a voltage ( $u_p$ ) to a piezoelectric actuator that changes the cavity length. This part of the Hamiltonian corresponds to the elementary building block of the recent ground-breaking experiments based on coupled 0D-polariton systems [22]. The second line of the Hamiltonian describes the Feshbach-like physics associated with the bound-molecular (trion) channel and the corresponding effective interactions between the excitons and the electrons [1]. Provided that the exciton-electron coupling can be treated as an attractive contact interaction,  $E_T$  directly determines the interaction strength  $V_q = V_0$  [23]. The Hamiltonian of Eq. (1) therefore combines the physics of cavity-polaritons with that of Fermi polarons.

The Fermi polaron problem describes the screening of a mobile impurity via generation of particle-hole pairs across the Fermi surface (Fig. 1c). When the impurity is a fermion with different spin, this problem corresponds to the highly polarized limit of a strongly interacting Fermi system [1]. The corresponding systems exhibit a wealth of complex phenomena, such as the elusive Fulde-Ferrell-Larkin-Ovchinnikov pairing mechanism, the Chandrasekar-Clogston limit of BCS superconductivity and itinerant ferromagnetism [24]. While the cavity spectroscopy we implement to study the exciton-2DES problem in the weak coupling regime is analogous to the rf spectroscopy of impurities in degenerate Fermi gases [2], the strong coupling regime of the TMD-

monolayer-microcavity system represents a new frontier for quantum impurity physics. More specifically, since the exciton-polariton dispersion can be tuned by changing  $\omega_c(u_p) - E_{exc}$  to yield an effective polariton mass that is (up to) four orders of magnitude smaller than that of the electron [6], the extension of our experiments to a 2D cavity could realize a Fermi-polaron system with a tunable ultra-small mass impurity. We find that a theoretical model based on a truncated basis approach (Chevy ansatz) [25] treating the system as an excitonic Fermi polaron captures the experimental signatures such as the  $n_e$ -dependent blueshift of the exciton resonance and the oscillator strength transfer from the repulsive exciton polaron to the attractive polaron [7].

We embed a MoSe<sub>2</sub>/hBN/graphene heterostructure [26] inside an open optical cavity [27] consisting of a flat dielectric mirror and a fiber-mirror with a radius of curvature of 30  $\mu\text{m}$  (Fig. 1a). We use the graphene layer as a top gate that controls the electron density in the MoSe<sub>2</sub> layer (Fig. 1b), allowing us to tune the Fermi energy from  $E_F = 0$  to  $E_F \geq E_T$ . The thickness of the hBN layer is chosen to ensure that the MoSe<sub>2</sub> is located at an anti-node of the cavity, while the graphene monolayer is at a node where the intra-cavity field vanishes; this choice ensures that the graphene absorption does not lead to a deterioration of the cavity finesse which we estimate to be  $\mathcal{F} \sim 200$ .

In order to characterize the elementary optical excitations of the MoSe<sub>2</sub> monolayer, we set the cavity length to  $L_{cav} = 9.1 \mu\text{m}$  and carry out spectroscopy in the limit of weak (perturbative) coupling to the cavity mode. Figure 2a depicts the cavity transmission spectrum in this weak coupling regime obtained for  $V_g = -3$  V: the parallel diagonal lines correspond to transmission maxima associated with neighboring axial modes of the cavity. Zooming in to the central mode, we find that the mode energy as well as its linewidth varies non-trivially due to coupling to the MoSe<sub>2</sub> excitations. We plot the color-coded cavity line broadening (Fig. 2b) and line-shift (Fig. 2c) as a function of  $V_g$  (vertical axis) and the fundamental cavity mode frequency (horizontal axis). Since the bare cavity linewidth ( $\sim 0.38$  meV) is much smaller than the spectral features associated with exciton-polaron and trion resonances, the increase in cavity linewidth, or shift in cavity resonance frequency allows us to determine the imaginary (absorption) and real (dispersion) parts of MoSe<sub>2</sub> linear susceptibility (Fig. 2b-c). We note that even for  $L_{cav} = 9.1 \mu\text{m}$ , the exciton resonance is in the strong coupling regime for  $V_g < -10$  V, albeit with a small normal mode splitting: in this limit, highlighted by the dashed rectangle in Fig. 2b, it is not possible to directly measure the cavity line broadening (see Supplementary Information). As a finite electron density  $n_e$  is introduced by increasing  $V_g$  to  $-10$  V, a new absorption resonance (shaded blue curve), which is red-detuned by  $\sim 25$  meV from the bare exciton reso-

nance, emerges (Fig. 2d). At the same time, the exciton line blueshifts and broadens, thereby ensuring that the coupling to the cavity mode is in the perturbative limit. For  $V_g = 0$  V, the exciton resonance sharply shifts to higher energies as the lower-energy resonance becomes prominent (Fig. 2e). Further increase in  $V_g$  leads to an increasing energy of the redshifted resonance and an indiscernible exciton feature (Fig. 2f). We observe that for  $V_g > 20$  V, the MoSe<sub>2</sub> monolayer-induced cavity line broadening exhibits a spectrally flat blue tail in absorption (Fig. 2g). Since the cavity line broadening (Fig. 2b) and line-shift (Fig. 2c) data are connected by Kramers-Kronig relations, we mainly refer to line broadening in the following discussion.

We note that TMD monolayer PL at low  $n_e$  is known to exhibit sharp trion peaks [26]: photo-excited carriers predominantly relax to the lowest energy molecular (trion) state, which in turn decays by spontaneous emission to an excited state of the 2DES. We observe that in Figure 2e the PL line (green curve) is only slightly redshifted with respect to the peak in absorption. In contrast, increasing  $V_g$  further results in a redshift of the PL peak while the low-energy absorption peak experiences a blueshift (Fig. 2f). Further increase in  $n_e$  results in a large splitting exceeding 40 meV between the absorption and PL peaks (Fig. 2g), suggesting that they are associated with different elementary optical excitations.

We identify the emerging lower-energy resonance in absorption for  $V_g \geq -10$  V as stemming from attractive-exciton-polarons (Fig. 1c). The observation of substantial line broadening of the cavity mode indicate a sizable overlap between the ground state (with no optical or electronic excitation above the Fermi sea) and the optically excited state. These observations in turn render it unlikely that the observed features are associated with direct optical excitation of a trion. In contrast to the latter, an attractive polaron has a finite amplitude for having no electron-hole pair excitation across the Fermi surface ensuring a sizable quasi-particle weight. The strong  $n_e$ -dependent blueshift of the exciton resonance in turn indicates that it should be identified as the repulsive polaron – a metastable excitation of the interacting electron-2DES system [3].

The most spectacular signature demonstrating the polaron nature of the absorption resonances is obtained in the strong coupling regime of the interacting cavity-exciton-electron system, which is reached by decreasing the effective cavity length to  $\sim 1.9 \mu\text{m}$ . Figure 3a-c shows the transmission spectrum as the cavity length is changed by  $\sim 100$  nm at three different gate voltages. The observation of normal mode splitting when the cavity mode is tuned into resonance with the lower-energy absorption resonance (Fig. 3b-c) demonstrates the large overlap between the initial and final states of this optical transition which in turn proves that the resonance is associated with the attractive-exciton-polaron. In contrast,

the trion transition should have vanishing overlap with the 2DES ground state and should not lead to strong coupling to the cavity. We quantify the relative transition strength of the attractive polaron and trion transitions in the discussion section where we detail the theoretical model we used. We also emphasize that the PL spectrum, which we associate with trion emission, shows no normal mode splitting for the parameters which yield split attractive-polaron-polariton peaks in transmission (Fig. 3f).

Figure 3d-f show cross sections through Figure 3a-c. The simultaneous appearance of polaritons in both the repulsive and attractive polaron branches (Fig. 3e) indicate that our experiments make it possible to study a new regime of polaron physics where an ultra-light polariton impurity is dressed with electron-hole pair excitations. An exciting future direction motivated by our observations is the investigation of polaron formation on polariton transport.

The emergence of the lower-energy resonance and the gradual disappearance of the exciton resonance as  $n_e$  is increased has been previously predicted and identified as oscillator strength transfer from the exciton to trion [7, 21]. To investigate how strong coupling alters the polaron formation and the associated oscillator strength transfer, we measured the normal mode splitting over a large range of  $V_g$ . Figure 4a shows, as a function of  $V_g$ , the transmission spectrum of the MoSe<sub>2</sub> monolayer when the bare cavity mode is in resonance with the repulsive-polaron (left) or the attractive-polaron. Increasing  $n_e$  results in decreasing (increasing) normal mode splitting for the repulsive (attractive) polaron. However, the maximum splitting for the attractive-polaron obtained for  $V_g \approx -5$  V is less than half as big as that of exciton obtained in the absence of a 2DEG. Further increase in  $V_g$ , or equivalently increase of  $n_e$ , results in diminishing normal mode splitting. In the latter limit, the optical oscillator strength is distributed over a broad energy range of order  $E_F$ , thereby suppressing the coupling to the narrow cavity mode.

For theoretical modeling we use the truncated basis method (see Supplementary Information), in which the Hilbert space is restricted to include at most a single electron-hole pair [28]. Although an impurity inside a Fermi sea scatters an infinite number of electron-hole pairs [29], this variational approach has been proven to be surprisingly accurate for modeling cold-atom systems, due to the destructive interference of higher order processes [30, 31]. Since the screened interaction between electrons and excitons is short ranged, we treat it as a contact interaction. In contrast to the cold-atom systems, the TMD-exciton-electron system has two types of excitons and Fermi seas distinguished by the valley pseudospin degree-of-freedom [9]. However, because at small Fermi-energies, the interaction between excitons and electrons inside the same valley is suppressed due to

Pauli exclusion, we neglect it altogether and model our system by a single excitonic impurity in K (-K) valley interacting with electrons in the -K (K) valley. We remark that electron-electron interactions can be neglected if we truncate the Hilbert space to just one electron-hole pair. We also take into account phase-space filling effects, which decrease the binding energy of the exciton and result in a blueshift of all quasi-particle energies by  $2E_F$ . This simple theoretical model captures some but not all of the experimental observations in MoSe<sub>2</sub>. Finally, we note that for WSe<sub>2</sub> and WS<sub>2</sub>, phase space filling should be absent and as a consequence the attractive (repulsive) polaron will exhibit a red (blue) shift [19].

We present the theoretical results in the weak-coupling regime in Figure 4b. As a function of  $E_F$  all resonances exhibit a blueshift in energy that stems from phase-space filling. The exciton resonance, which dominates the spectrum for vanishing  $E_F$ , exhibits a further blueshift with increasing  $E_F$ , justifying its identification as the repulsive polaron. For  $E_F > 0$ , a lower-energy attractive polaron branch, with an energy comparable to the molecule/trion energy, emerges [23]. In contrast to the experimental results, our simple theoretical model shows an abrupt turn-on of the blueshift of the repulsive polaron branch for small  $E_F$ : this discrepancy possibly stems from the disorder in the flake that results in localized electronic states below the conduction band edge. We also capture the quasi-particle weight transfer from the repulsive polaron to the attractive polaron and the broadening of the repulsive polaron. Our model also predicts a trion-hole continuum of width  $2/3E_F$ , of very small weight. Figure 4c shows that the quasi-particle weight of the trion-hole continuum remains smaller than that of the attractive polaron branch by a factor of 10, supporting our claim that the polariton formation cannot be associated with trions due to the small overlap between the latter and the 2DES ground state + one cavity-photon. In contrast to the negatively-charged trion, a Fermi polaron described by the Chevy ansatz corresponds to a neutral excitation, consisting of a Fermi-sea electron-hole pair bound to an exciton [28].

In our model, the  $k = 0$  trion is always higher in energy than the attractive polaron. An extended truncated basis approach, which includes states containing a molecule accompanied by an electron-hole pair, can be used to show that the  $k = 0$  trion state should be lower in energy for  $E_F < 5$  meV [23]. In contrast to the experimental findings, we cannot capture correctly the broadening of the attractive polaron, since we have not considered an ansatz with an extra electron-hole pair. Figure 4d shows the calculated spectral function in the strong-coupling regime. We see that the polaron peaks become sharper due to the coupling to the narrow cavity. We notice that we capture the decrease (increase) in the light matter coupling for the attractive (repulsive) polarons as  $E_F$  increases. However, our model does not predict the full dis-

appearance of the repulsive (or attractive) polaron strong coupling to the cavity. Theoretically, at  $E_F = 30$  meV the normal mode splitting of the repulsive polaron is reduced to 7 meV while the normal mode splitting of the attractive polaron is roughly 13 meV. The discrepancies between the experimental data and the theoretical predictions may also stem from our approximation of a rigid exciton: our model does not capture exchange and correlation effects which are known to play a role in trion formation [7].

Our experiments establish strongly bound excitons in TMD monolayers, simultaneously embedded in a 2DES and a microcavity, as a new paradigm for quantum impurity and polaron physics. In stark contrast to prior work, we identify the optical excitations that are accessible in resonant spectroscopy as repulsive and attractive exciton polarons and polaron-polaritons, which are simultaneously present for Fermi energies that are smaller than the molecular (trion) binding energy. For  $E_F$  exceeding the conduction band spin-orbit coupling, TMD monolayers exhibit both intra- and inter-valley trions that are coupled by electron-hole exchange [32]: an interesting open question is whether the Berry curvature of the corresponding exchange coupled intra- and inter-valley attractive polarons leads to novel transport signatures. While we report the measurement of the spectral function of the interacting polariton-2DES system, we highlight that it is possible to directly measure the nonequilibrium response of the system in the time domain using ultrashort laser pump-probe spectroscopy in the regime  $E_F \leq 10$  meV. Finally, another interesting extension of our work would be the investigation of a Bose-polaron problem where an optically injected -K valley polariton impurity interacts with Bogoliubov excitations out of a polariton condensate in the +K valley.

**Acknowledgements** J. Reichel, A. Kis and R. Schmidt have made invaluable contributions to the experimental and theoretical aspects of this work. The authors also acknowledge many insightful discussions with C. Ciuti, M. Combescot, M. Fleischhauer, L. Glazman, M. Goldstein, F. Grusdt, D. Pimenov and J. von Delft. This work is supported by an ERC Advanced investigator grant (POLTDES), Harvard-MIT CUA, NSF Grant No. DMR-1308435, Dr. Max Rössler, the Walter Haefner Foundation and the ETH Foundation.

- 
- [1] P. Massignan, M. Zaccanti, and G. M. Bruun, Reports on Progress in Physics **77**, 034401 (2014).
- [2] A. Schirotzek, C.-H. Wu, A. Sommer, and M. W. Zwierlein, Phys. Rev. Lett. **102**, 230402 (2009), URL <http://link.aps.org/doi/10.1103/PhysRevLett.102.230402>.
- [3] R. Schmidt, T. Enss, V. Pietilä, and E. Demler, Phys. Rev. A **85**, 021602 (2012), URL <http://link.aps.org/doi/10.1103/PhysRevA.85.021602>.
- [4] C. Kohstall, M. Zaccanti, M. Jag, A. Trenkwalder, P. Massignan, G. M. Bruun, F. Schreck, and R. Grimm, Nature **485**, 615 (2012).
- [5] M. Koschorreck, D. Pertot, E. Vogt, B. Fröhlich, M. Feld, and M. Köhl, Nature **485**, 619 (2012).
- [6] I. Carusotto and C. Ciuti, Reviews of Modern Physics **85**, 299 (2013).
- [7] A. Esser, R. Zimmermann, and E. Runge, Physica Status Solidi B Basic Research **227**, 317 (2001).
- [8] B. Ganchev, N. Drummond, I. Aleiner, and V. Falko, Physical review letters **114**, 107401 (2015).
- [9] X. Xu, W. Yao, D. Xiao, and T. Heinz, Nature Physics **10**, 343 (2014).
- [10] X. Liu, T. Galfsky, Z. Sun, F. Xia, E.-c. Lin, S. Lee, Yi-Hsien Kena-Cohen, and V. M. Menon, Nature Photonics **9**, 30 (2015).
- [11] F. Withers, O. Del Pozo-Zamudio, A. Mishchenko, A. Rooney, A. Gholinia, K. Watanabe, T. Taniguchi, S. Haigh, A. Geim, and A. Tartakovskii, Nature Communications **6** (2015).
- [12] F. P. Laussy, A. V. Kavokin, and I. A. Shelykh, Physical review letters **104**, 106402 (2010).
- [13] O. Cotlet, S. Zeytinoglu, M. Sigrist, E. Demler, and A. Imamoglu, arXiv preprint arXiv:1510.02001 (2015).
- [14] A. Chernikov, T. C. Berkelbach, H. M. Hill, A. Rigosi, Y. Li, O. B. Aslan, D. R. Reichman, M. S. Hybertsen, and T. F. Heinz, Phys. Rev. Lett. **113**, 076802 (2014), URL <http://link.aps.org/doi/10.1103/PhysRevLett.113.076802>.
- [15] A. Srivastava and A. Imamoglu, Phys. Rev. Lett. **115**, 166802 (2015), URL <http://link.aps.org/doi/10.1103/PhysRevLett.115.166802>.
- [16] J. Zhou, W.-Y. Shan, W. Yao, and D. Xiao, Phys. Rev. Lett. **115**, 166803 (2015), URL <http://link.aps.org/doi/10.1103/PhysRevLett.115.166803>.
- [17] G. Wang, I. C. Gerber, L. Bouet, D. Lagarde, A. Balocchi, M. Vidal, T. Amand, X. Marie, and B. Urbaszek, 2D Materials **2**, 045005 (2015), URL <http://stacks.iop.org/2053-1583/2/i=4/a=045005>.
- [18] T. C. Berkelbach, M. S. Hybertsen, and D. R. Reichman, Phys. Rev. B **88**, 045318 (2013), URL <http://link.aps.org/doi/10.1103/PhysRevB.88.045318>.
- [19] A. Chernikov, A. M. van der Zande, H. M. Hill, A. F. Rigosi, A. Velauthapillai, J. Hone, and T. F. Heinz, Phys. Rev. Lett. **115**, 126802 (2015), URL <http://link.aps.org/doi/10.1103/PhysRevLett.115.126802>.
- [20] R. Rapaport, E. Cohen, A. Ron, E. Linder, and L. N. Pfeiffer, Phys. Rev. B **63**, 235310 (2001), URL <http://link.aps.org/doi/10.1103/PhysRevB.63.235310>.
- [21] S. Smolka, W. Wuester, F. Haupt, S. Faelt, W. Wegscheider, and A. Imamoglu, Science **346**, 332 (2014).
- [22] T. Jacqmin, I. Carusotto, I. Sagnes, M. Abbarchi, D. D. Solnyshkov, G. Malpuech, E. Galopin, A. Lemaître, J. Bloch, and A. Amo, Phys. Rev. Lett. **112**, 116402 (2014), URL <http://link.aps.org/doi/10.1103/PhysRevLett.112.116402>.
- [23] M. M. Parish, Physical Review A **83**, 051603 (2011).
- [24] R. Duine and A. MacDonald, Physical review letters **95**, 230403 (2005).
- [25] M. M. Parish and J. Levinsen, Physical Review A **87**, 033616 (2013).
- [26] J. S. Ross, S. Wu, H. Yu, N. J. Ghimire, A. M. Jones, G. Aivazian, J. Yan, D. Mandrus, David G. and Xiao, W. Yao, and X. Xu, Nature Communications **4** (2015).

- [27] B. Besga, C. Vanepf, J. Reichel, J. Estève, A. Reinhard, J. Miguel-Sanchez, A. Imamoglu, and T. Volz, *Phys. Rev. Applied* **3**, 014008 (2015), URL <http://link.aps.org/doi/10.1103/PhysRevApplied.3.014008>.
- [28] R. A. Suris, *Optical Properties of 2D Systems with Interacting Electrons* (Springer Netherlands, Dordrecht, 2003), chap. Correlation Between Trion and Hole in Fermi Distribution in Process of Trion Photo-Excitation in Doped QWs, pp. 111–124, ISBN 978-94-010-0078-9, URL [http://dx.doi.org/10.1007/978-94-010-0078-9\\_9](http://dx.doi.org/10.1007/978-94-010-0078-9_9).
- [29] P. W. Anderson, *Physical Review Letters* **18**, 1049 (1967).
- [30] J. Vlietinck, J. Ryckebusch, and K. Van Houcke, *Physical Review B* **87**, 115133 (2013).
- [31] R. Combescot and S. Giraud, *Physical review letters* **101**, 050404 (2008).
- [32] H. Yu, G.-B. Liu, P. Gong, X. Xu, and W. Yao, *Nature Communications* **5** (2014).

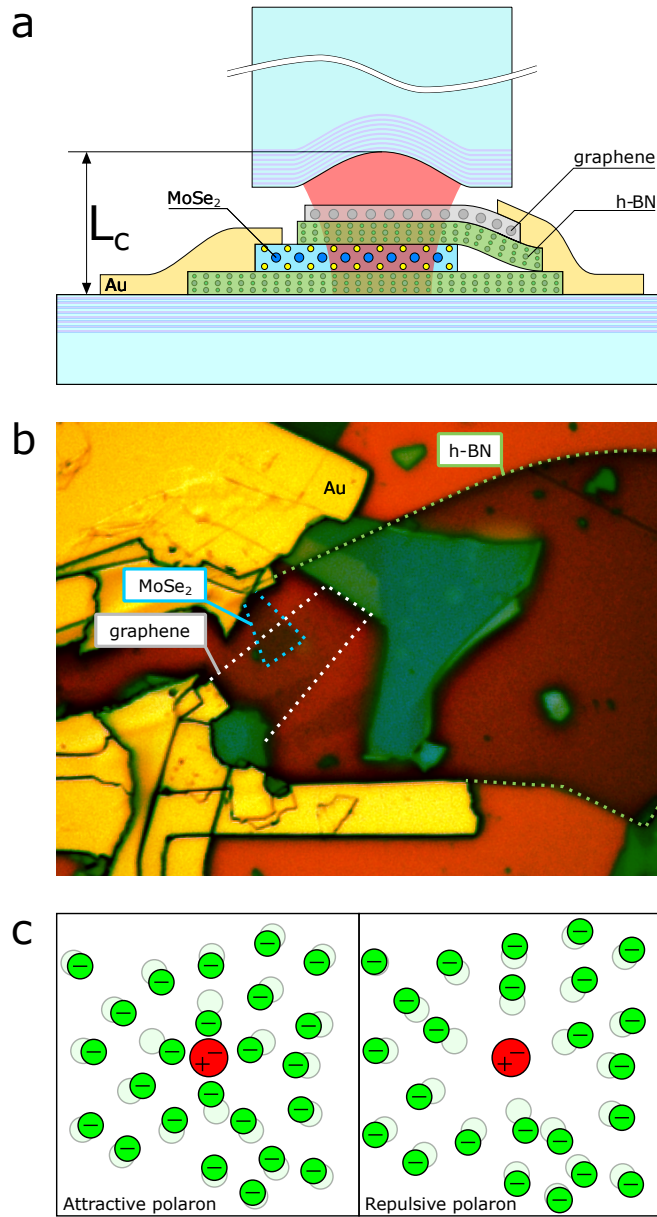


FIG. 1. **A MoSe<sub>2</sub>/hBN/graphene heterostructure in a fiber cavity.** **a**, The sample consists of a  $3\ \mu\text{m}$  by  $5\ \mu\text{m}$  MoSe<sub>2</sub> monolayer sandwiched between 10nm and 110nm thick hBN layers. A graphene layer on top completes the heterostructure that allows for controlling the electron density in the MoSe<sub>2</sub> monolayer by gating. The heterostructure is placed on top of a flat dielectric mirror (DBR). The thicknesses of the hBN layers are chosen to ensure that the MoSe<sub>2</sub> monolayer is at an antinode and the graphene layer is at a node of the cavity formed by the bottom dielectric mirror and the top fiber mirror. The finesse of the cavity is  $\sim 200$ ; the cavity length can be tuned from  $1.9\ \mu\text{m}$  to  $15\ \mu\text{m}$ . **b**, The optical microscope image of the heterostructure where the overlap between the MoSe<sub>2</sub> monolayer and the top graphene layer is identified. **c**, Due to exciton-electron interactions, the exciton is surrounded by an electron screening cloud that leads to the formation of an attractive polaron (left panel). For a repulsive polaron the electrons are pushed away from the exciton leading to a higher energy metastable excitation (right panel).

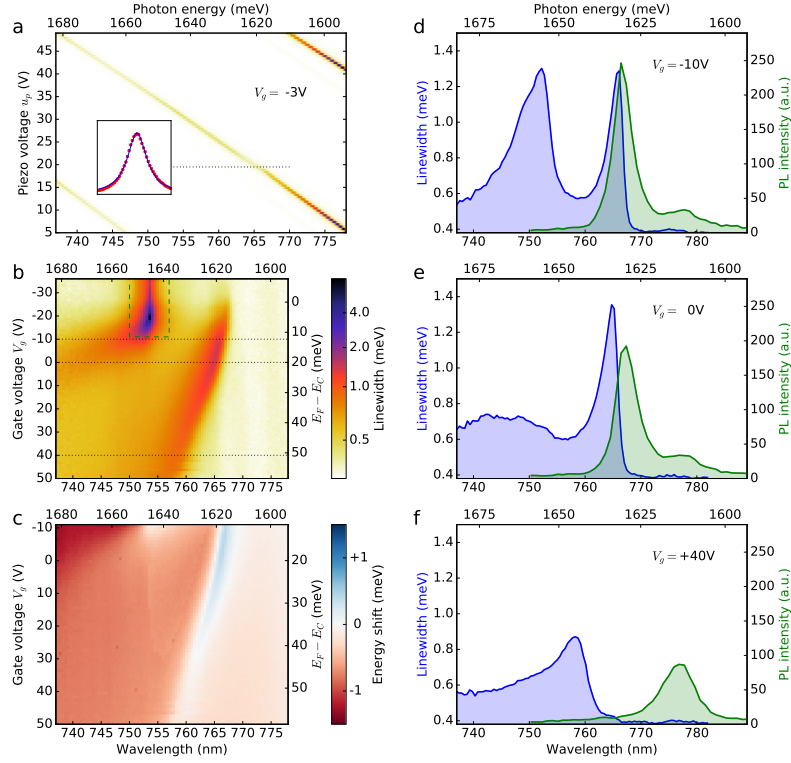


FIG. 2. **Cavity spectroscopy of the interacting exciton-electron system in the weak coupling regime.** **a**, The white light transmission spectrum of the fiber cavity incorporating the MoSe<sub>2</sub>/hBN/graphene heterostructure, as a function of the piezo voltage (vertical scale) that is varied to tune the cavity frequency. Since the bare cavity linewidth of 0.3meV is much smaller than all other energy scales, cavity transmission allows for identifying the linear optical response of the heterostructure: Whenever the cavity mode is at a frequency absorbed by the MoSe<sub>2</sub> flake, its linewidth increases. Consequently, the MoSe<sub>2</sub> absorption spectrum can be measured as a frequency dependent broadening of the cavity. The insert shows the cavity transmission at  $V_g = -3$  V and  $u_p = 20$  V fitted with a lorentzian curve. **b**, The MoSe<sub>2</sub> absorption spectrum determined by measuring the enhancement of the cavity linewidth for each cavity frequency (horizontal axis) and gate voltage or equivalently the Fermi energy (vertical axis). When the Fermi energy is below the conduction band minimum ( $E_C$ , we choose  $E_C = 0$ ), absorption is only observed at the bare exciton frequency. As electrons are introduced, the exciton resonance experiences a sharp blueshift together with broadening. Concurrently, there is a new resonance emerging at  $\sim 25$  meV below the bare exciton energy. **These features are identified as the repulsive and attractive exciton-polaron resonances.** For  $V_g < -10$  V, the exciton and the cavity mode are in the strong-coupling regime (the region highlighted using the dashed rectangle) and it is not possible to directly extract imaginary part of the MoSe<sub>2</sub> linear susceptibility: in this regime, we measure and plot the linewidth of the cavity-like polariton. **c**, The measured real part of the susceptibility of the MoSe<sub>2</sub> flake as a function of the cavity frequency (horizontal axis) and the gate voltage (vertical axis). The data presented here is connected to the absorption data of Fig. 2b via Kramers-Kroenig relations. In the absence of the MoSe<sub>2</sub> flake, there is an expected change of the cavity resonance (peak in the spectrum of the transmitted light) with changing piezo voltage. In the presence of MoSe<sub>2</sub>, the index of refraction seen by the photons is modified due to the real part of the MoSe<sub>2</sub> susceptibility, thereby modifying the effective cavity length and leading to a shift of the cavity resonance wavelength as compared to what we would have obtained in the absence of MoSe<sub>2</sub>. **d**, Line-cut through the cavity line broadening data (blue shaded curve) for  $V_g = -10$  V: both repulsive and attractive polaron features are visible. We expect the trion and attractive-polaron energies to be comparable for this  $V_g$ . The photoluminescence (PL) data is shown in green. **e**, Line-cut through the cavity line broadening and shift data for  $V_g = 0$  V: the line broadening/absorption data is dominated by the attractive polaron which is now blue-shifted with respect to the trion PL. **f**, Line-cut through the cavity line broadening and shift data for  $V_g = 40$  V: the PL and absorption peaks are separated from each other by 40 meV suggesting that PL and absorption data stem from different quasiparticles, namely the trion and the attractive polaron, respectively.

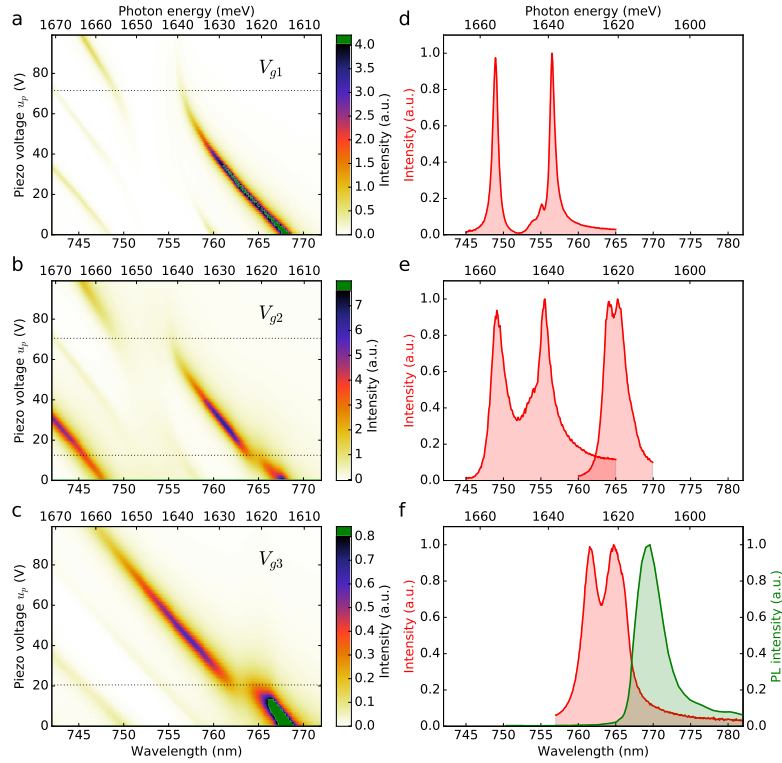


FIG. 3. **Cavity spectroscopy of the interacting exciton-electron system in the strong coupling regime.** **a**, The white light transmission spectrum as a function of the piezo voltage (vertical scale) for an average cavity length of  $1.9 \mu\text{m}$ . Due to enhanced cavity electric field, the interaction between the cavity mode and MoSe<sub>2</sub> resonances is directly observed in cavity transmission spectra as anticrossings associated with polariton formation. For gate voltages where the MoSe<sub>2</sub> monolayer is devoid of electrons ( $V_{g1}$ ) the spectrum shows a prominent anticrossing with a normal mode splitting of 16 meV. The elementary optical excitations in this regime are bare exciton-polaritons without any polaron effect. The green area indicates values outside the range of the colormap. **b**, White light transmission spectrum for  $V_g = V_{g2} = -5$  V, showing two anticrossings associated with the formation of repulsive- and attractive-polaron-polaritons. **The observation of anticrossings for both lower and higher energy resonances proves that these originate from Fermi-polarons with a large quasiparticle weight.** **c**, White light spectrum for a higher gate voltage ( $V_{g3}$ ), where only the attractive-polaron exhibits non-perturbative coupling to the cavity mode. **d** Line-cut through the data in Fig. 3a for the piezo voltage  $u_p = 72$  V shows the transmission spectrum (red curve) at the resonance of the cavity with the exciton. **e**, Line-cut through the data in Fig. 3b for the piezo voltage  $u_p = 13$  V respectively  $u_p = 71$  V. **f** Line-cut through the data in Fig. 3e for  $u_p = 21$  V, corresponding to the case where the cavity mode is resonant with the attractive polaron resonance. The photoluminescence spectrum in the strong coupling regime is also plotted (green shaded curve).



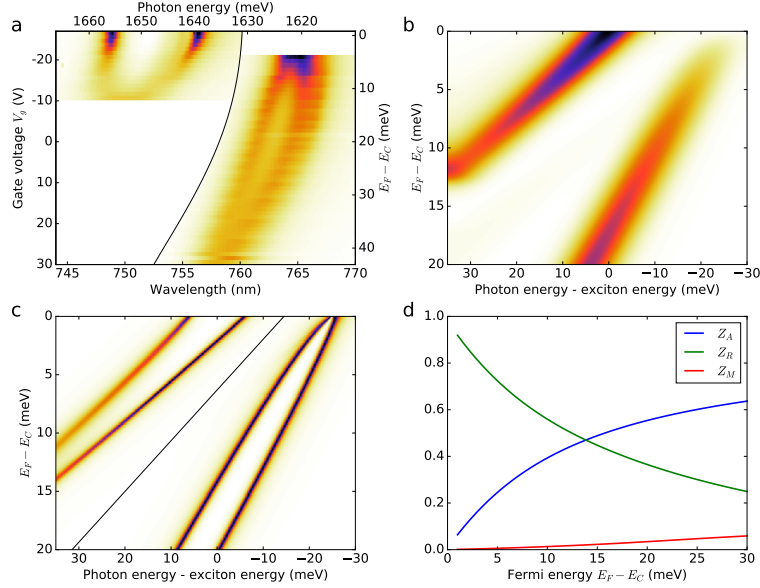


FIG. 4. **Competition between repulsive and attractive polaron resonances.** **a**, The white light transmission spectrum of the fiber cavity incorporating the MoSe<sub>2</sub>/hBN/graphene heterostructure, as a function of the gate voltage (vertical scale) for two different settings of the cavity length: the left (right) part shows the transmission when the cavity is tuned on resonance with the repulsive (attractive) polaron. For each horizontal line, the cavity frequency is tuned so as to yield two polariton modes with equal peak amplitude. As  $V_g$  is increased, the oscillator strength transfer from the repulsive to attractive branch is clearly visible. While the normal mode splitting for the repulsive branch disappears for  $V_g \simeq -10$  V, the collapse of the splitting takes place at  $V_g = 25$  V for the attractive branch. **b**, The spectral function calculated using the Chevy ansatz in the weak coupling regime is in good qualitative agreement with the absorption spectra of Fig. 2b. **c**, The calculated quasi-particle weights showing the oscillator strength transfer from the repulsive to the attractive polaron as the Fermi energy is increased. The weight of the trion+hole continuum increases linearly with the Fermi energy but remains less than 0.1 even for Fermi energies exceeding the trion binding energy. **d**, The spectral function calculated using the Chevy ansatz in the strong coupling regime captures the oscillator strength transfer from the repulsive to attractive polaron depicted in Fig. 4a but fails to predict the collapse of the normal mode splitting with increasing electron density.

**SUPPLEMENTARY MATERIALS: FERMION POLARON-POLARITONS IN CHARGE-TUNABLE  
ATOMICALLY THIN SEMICONDUCTORS**

**THEORY**

Although in the experiments we have a 0D cavity, these experiments can be extended to a system with a 2D cavity. Therefore, in the theory section we will analyse the latter case. The 0D cavity case will appear as a special case of our result. However, in considering a 2D cavity we show that ultra-low mass polarons can easily be obtained experimentally by exchanging the 0D cavity with the 2D cavity.

We start from the following Hamiltonian:

$$H = \sum_k \omega_C(k) c_k^\dagger c_k + \sum_k \omega_X(k) x_k^\dagger x_k + \sum_k g(c_k^\dagger x_k + h.c.) + \sum_k \epsilon(k) e_k^\dagger e_k + \sum_{k,k',q} V_q x_{k+q}^\dagger e_{k'-q}^\dagger e_{k'} x_k \quad (S1)$$

$$\omega_C(k) = \frac{\hbar k^2}{2m_c}, \quad \omega_X(k) = \frac{\hbar k^2}{2m_{exc}} + 2E_F, \quad \epsilon_k^{(e)} = \frac{\hbar k^2}{2m_e}, \quad (S2)$$

where  $c, x$  and  $e$  are the destruction operators of a cavity photon, an exciton and an electron respectively, while  $m_c, m_{exc}$  and  $m_e$  are the masses of the cavity photon, the exciton and the electron. The third term corresponds to the coupling between excitons and the cavity field, while the last term incorporates the interaction between the exciton and the Fermi sea. Although we consider the exciton to be a rigid object, the interaction between the exciton and the Fermi sea contains the effects due to electron exchange between the exciton and the Fermi sea. The  $2E_F$  term in the exciton dispersion is due to phase space filling which results in an overall blueshift of the exciton line.

**Chevy ansatz for the polaron**

In order to analyze the problem we make a Chevy-type ansatz [S1] for the polaron state, which truncates the Hilbert space to a single electron-hole pair:

$$|\Psi^{(p)}\rangle = \left( \phi_0 x_p + \varphi_0 c_p + \sum_{k,q} \phi_{k,q} x_{p+q-k}^\dagger e_k^\dagger e_q + \sum_{k,q} \varphi_{k,q} c_{p+q-k}^\dagger e_k^\dagger e_q \right) |0\rangle, \quad (S3)$$

where we defined the vacuum  $|0\rangle$  as an undisturbed Fermi sea and no excitons in the system. This ansatz takes into account the total momentum conservation in our system and describes a quasi particle of momentum  $p$  formed by the superposition of a cavity photon and an exciton dressed by an electron-hole pair from the Fermi sea. To obtain the ground-state we must minimize the quantity  $\langle \Psi^{(p)} | E - H | \Psi^{(p)} \rangle$ :

$$\langle \Psi^{(p)} | E - H | \Psi^{(p)} \rangle = E \left( |\phi_0|^2 + |\varphi_0|^2 + \sum_{k,q} |\phi_{k,q}|^2 + \sum_{k,q} |\varphi_{k,q}|^2 \right) - H_{\text{var}}^{(p)} \quad (S4)$$

$$\begin{aligned} H_{\text{var}}^{(p)} = \langle \Psi^{(p)} | H | \Psi^{(p)} \rangle &= \omega_X(p) |\phi_0|^2 + \omega_C(p) |\varphi_0|^2 + \sum_{k,q} E_X(p, k, q) |\phi_{k,q}|^2 + \sum_{k,q} E_C(p, k, q) |\varphi_{k,q}|^2 \\ &- g \left[ \phi_0^* \varphi_0 + \sum_{k,q} \phi_{k,q}^* \varphi_{k,q} + c.c. \right] + |\phi_0|^2 \sum_q V_0 + \sum_{k,q} [\phi_0^* \phi_{k,q} V_{k-q} + c.c.] \\ &+ \sum_{k,q,k'} [\phi_{k,q}^* \phi_{k',q} V_{k-k'} + c.c.] - \sum_{k,q,q'} [\phi_{k,q}^* \phi_{k,q'} V_{q-q'} + c.c.], \end{aligned} \quad (S5)$$

where  $E_X(p, k, q) \equiv \omega_X(p+q-k) + \epsilon(k) - \epsilon(q)$  and  $E_C(p, k, q) \equiv \omega_C(p+q-k) + \epsilon(k) - \epsilon(q)$ . Each term in  $H_{\text{var}}$  corresponds to a physical process allowing the observation of the competition between different processes, in trying to minimize  $H_{\text{var}}$  subject to the normalization constraint. Minimizing the above equation, we obtain the following

equations:

$$\omega_C(p)\varphi_0 - g\phi_0 = E\varphi_0 \quad (\text{S6})$$

$$E_C(p, k, q)\varphi_{k,q} - g\phi_{k,q} = E\phi_{k,q} \quad (\text{S7})$$

$$\omega_X(p)\phi_0 - g\varphi_0 + \sum_q \phi_0 V_0 + \sum_{k,q} \phi_{k,q} V_{k-q} = E\phi_0 \quad (\text{S8})$$

$$E_X(p, k, q)\phi_{k,q} - g\varphi_{k,q} + V_{k-q}\phi_0 + \sum_{k'} V_{k'-k}\phi_{k',q} + \sum_{q'} V_{q'-q}\phi_{k,q'} = E\phi_{k,q}. \quad (\text{S9})$$

Because the cavity coupling does not mix different momentum states, we can eliminate the first two equations and obtain a set of two equations:

$$\left( \omega_X(p) - \frac{g^2}{\omega_C(p)} \right) \phi_0 + \sum_q \phi_0 V_0 + \sum_{k,q} \phi_{k,q} V_{k-q} = E\phi_0 \quad (\text{S10})$$

$$\left( E_X(p, k, q) - \frac{g^2}{E_C(p, k, q)} \right) \phi_{k,q} + V_{k-q}\phi_0 + \sum_{k'} V_{k'-k}\phi_{k',q} + \sum_{q'} V_{q'-q}\phi_{k,q'} = E\phi_{k,q}. \quad (\text{S11})$$

Notice that the effect of the cavity is to renormalize the energies of many body states. The correction is recognized as the exact self-energy due to interactions with the cavity field.

At this point it is straightforward to solve the problem by discretizing the momenta  $k, q$  and transforming the above equations into a matrix equation.

However, we can make further analytical progress by making a few reasonable approximations. First of all, we notice that the exciton-electron interaction is a Van-der-Waals interaction which decays as  $r^{-4}$  at large distances, with a range given by the Bohr radius  $a_B$  of the excitation. Including the screening effects due to the electron system, the interaction will become even shorter range. Therefore, at least for small Fermi energies (i.e.  $a_B k_F \ll 1$ ) we can approximate the interaction with a contact interaction which is constant  $V_k = V$  up to a cutoff  $\Omega$ . Since in two dimensions, an attractive potential always has a bound state of energy, in our case we denote it by  $-E_T$ , we can express the interaction strength as a function of the bound state energy and an ultraviolet cutoff:

$$\frac{1}{V} = - \sum_{k=0}^{\Omega} \frac{1}{E_T - \omega_X(0) + \omega_X(k) + \epsilon(k)}. \quad (\text{S12})$$

Since the physics should not depend on the ultraviolet cutoff, in the end we will let  $\Omega \rightarrow \infty$  and therefore  $V \rightarrow 0$ . As we will show a posteriori,  $\phi_{k,q} \sim 1/k^2$  for large  $k$ , which in turn implies that the last term on the left hand side vanishes when  $V \rightarrow 0$ . We will therefore proceed by neglecting this term.

We introduce the function  $\chi_q = \phi_0 + \sum_k \phi_{k,q}$ . In terms of this function:

$$\phi_0 = \frac{V \sum_q \chi_q}{E - \omega_X(p) + \frac{g^2}{\omega_C(p)}} \quad (\text{S13})$$

$$\phi_{k,q} = \frac{V \chi_q}{E - E_X(p, k, q) + \frac{g^2}{E_C(p, k, q)}}. \quad (\text{S14})$$

Reintroducing the above into the definition of  $\chi_q$  we can obtain the following self-consistent equation:

$$E = \omega_X(p) + \frac{g^2}{E - \omega_C(p)} + \sum_q \left[ \sum_{k=0}^{\Omega} \frac{1}{E_T - \omega_X(0) + \omega_X(k) + \epsilon(k)} - \sum_{k=k_F}^{\Omega} \frac{1}{E - E_X(p, k, q) + \frac{g^2}{E - E_C(p, k, q)}} \right]^{-1} \quad (\text{S15})$$

To gain further insight into the above equation we introduce the dispersion resulting from linearly coupling two harmonic oscillator modes of energies  $E_X(p, k, q)$  and  $E_C(p, k, q)$  with a coupling strength  $g_c$ . These resemble the polariton modes:

$$\Omega_{LP,UP}(p, k, q) = \frac{1}{2} \left[ E_X(p, k, q) + E_C(p, k, q) \pm \sqrt{(E_X(p, k, q) - E_C(p, k, q))^2 + 4g_c^2} \right]. \quad (\text{S16})$$

We also introduce the factors resembling the exciton fractions in polaritons. which show how much of the initial modes is contained in the new modes:

$$|X(p, k, q)|^2 = \frac{1}{2} \left( 1 + \frac{E_C(p, k, q) - E_X(p, k, q)}{\sqrt{(E_C(p, k, q) - E_X(p, k, q))^2 + 4g_c^2}} \right). \quad (\text{S17})$$

With the above notation we can rewrite the self consistent equation as:

$$E - \omega_X(p) = \frac{g^2}{E - \omega_C(p)} + \sum_q \left[ \sum_{k=0}^{\Omega} \frac{1}{E_T - \omega_X(0) + \omega_X(k) + \epsilon(k)} - \sum_{k=k_F}^{\Omega} \left( \frac{|X(p, k, q)|^2}{E - \Omega_{LP}(p, k, q)} + \frac{1 - |X(p, k, q)|^2}{E - \Omega_{UP}(p, k, q)} \right) \right]^{-1}. \quad (\text{S18})$$

We can simplify things further by noting that for  $p + q - k > k_{ph}$  ( $k_{ph}$  is of the order of the photon momentum and approximately given by  $\hbar k_{ph}^2 / (2m_c) = g_c$ )  $X(p, k, q) \approx 1$  and  $\Omega_{LP}(p, k, q) \approx E_X(p, k, q)$ . Since  $k_{ph}$  is much smaller than all the other momentum scales the phase space where these approximations break down is extremely small. Based on this phase-space argument we can simplify the above equation:

$$E = \omega_X(p) + \frac{g^2}{E - \omega_C(p)} + \sum_q \left[ \sum_{k=0}^{\Omega} \frac{1}{E_T - \omega_X(0) + \omega_X(k) + \epsilon(k)} - \sum_{k=k_F}^{\Omega} \frac{1}{E - E_X(p, k, q)} \right]^{-1} \quad (\text{S19})$$

We would have obtained the same equation if we started from an ansatz which did not contain the states corresponding to a photon dressed by an electron-hole pair (i.e.  $\varphi_{k,q} = 0$ ). Our full derivation serves to justify this approximation. We remark that the poles in the  $q$  summation correspond to the molecular energies that are obtained when choosing an ansatz of the form  $|\Phi^{(p)}\rangle = \phi_k x_{p-k}^\dagger e_k^\dagger e_p |0\rangle$ .

It can be shown that by replacing  $E \rightarrow E + i\eta$  ( $\eta \rightarrow 0^+$ ), the last term on the right hand side of the above equation is the self-energy of an exciton interacting with a Fermi sea. Although the inclusion of the infinitesimal  $i\eta$  might seem arbitrary at this point, it can be shown that it emerges from choosing a time dependent ansatz, and instead of minimizing  $\langle \Phi | H | \Phi \rangle$ , minimizing the action  $S = \int \langle \Phi(t) | i\partial/\partial t - H | \Phi(t) \rangle$  [S2]. Therefore, the above equation can be written more intuitively as:

$$E = \omega_X(p) + \Sigma_X(E, p) \quad (\text{S20})$$

$$\Sigma_X(E, p) = \Sigma_{X-C}(E, p) + \Sigma_{X-e}(E, p) \quad (\text{S21})$$

$$\Sigma_{X-C}(E, p) = \frac{g^2}{E - \omega_C(p)} \quad (\text{S22})$$

$$\Sigma_{X-e}(E, p) = \sum_q \left[ \sum_{k=0}^{\Omega} \frac{1}{E_T - \omega_X(0) + \omega_X(k) + \epsilon(k)} - \sum_{k=k_F}^{\Omega} \frac{1}{E + i\eta - E_X(p, k, q)} \right]^{-1} \quad (\text{S23})$$

In the above we made explicit the self energy of the exciton interacting with the cavity mode ( $\Sigma_{X-C}$ ) and with the electrons in the Fermi sea ( $\Sigma_{X-e}$ ).

Having found the self-energy of the exciton, we can also obtain the self-energy of the cavity photon:

$$\Sigma_C(E, p) = \frac{g^2}{E - \omega_X(p) - \Sigma_{X-e}(E, p)} \quad (\text{S24})$$

### Spectral Function

In the weak-coupling regime, in our experiment, we are probing the exciton spectral function:

$$A(t) = \langle 0 | x_0 e^{-iHt} x_0^\dagger | 0 \rangle \quad (\text{S25})$$

In the truncated basis the Fourier transform of the spectral function is given by:

$$A(\omega) = \frac{1}{\pi} \text{Im} \left[ \frac{1}{\omega + i\eta - \omega_0^{(x)} - \Sigma_X(\omega, 0)} \right] \quad (\text{S26})$$

In the strong coupling regime we are probing the spectral function of the cavity photon and therefore, in the above we should replace  $\Sigma_X$  with  $\Sigma_C$ .

In simulating the experimental results we choose a lifetime broadening of the exciton/photon linewidth of  $\eta = 1.0$  meV. Since the exciton is also subject to disorder broadening, in the weak coupling regime we convolve the resulting spectral function with a Gaussian kernel with a standard deviation of 14 meV (such that FWHM = 7 meV), obtained from fitting the experimental exciton line at zero Fermi energy.

### Polaron mass

Having found the exciton self-energy we can also determine the effective mass of the exciton due to the interaction with the light cavity photon and the electron system. Assuming that the lowest energy state is at energy  $E_0$  and momentum 0, the effective mass is given by:

$$\frac{1}{m^*} = \frac{1}{m_x} + \frac{\partial}{\partial^2 p} \Sigma_X(E_0, p) \Big|_0 = \frac{1}{m_x} + \frac{1}{m_c} + \frac{\partial}{\partial^2 p} \Sigma_{X-e}(E_0, p) \Big|_0 \quad (\text{S27})$$

Regardless of the contribution of the last term in the above equation we can see that, due to the small mass of the cavity photon, the polaron mass is going to be ultra-small. Therefore, we conclude that we are dealing with an ultra-low mass polaron. We emphasize that an ultra-low mass polaron can only be achieved by dressing a (polariton) impurity which is a superposition of an ultra-low mass particle (cavity photon) with a relatively heavy particle (exciton). Such a mixed-impurity exhibits an ultra-small mass for low momenta but restricts the recoil energy to the coupling energy  $g_c$ . Otherwise, if we did not have the relatively heavy particle, the dressing of an ultra-low mass impurity is very ineffective since  $E_T \rightarrow 0$  for the same  $V$ . This means that the impurity will not be affected by the Fermi sea at all.

## SAMPLE PREPARATION AND MEASUREMENT SETUP

The heterostructure studied in this work was assembled using the pickup technique [S3]: Flakes of the constituent materials are exfoliated onto separate substrates and sequentially picked up with a polycarbonate layer which finally deposits the complete heterostructure onto the target substrate. The target substrate in this case is a distributed Bragg reflector (DBR) ion beam sputtered onto a fused silica substrate. The DBR is designed to have a reflectivity of  $> 99.3\%$  for the spectral range of 680-800 nm and an intensity maximum at the DBR surface. The graphene top gate as well as the MoSe<sub>2</sub> flake were contacted using metal gates consisting of a thin layer of titanium followed by a thicker layer of gold. In order to increase the chance of a good contact to the MoSe<sub>2</sub> flake, a parallel contact via a second graphene flake was made.

The top mirror is formed by a dimple with radius of curvature of 30  $\mu\text{m}$  shot into the fiber facet with a CO<sub>2</sub> laser. The geometry of the dimple was measured with interferometry. The fiber facet was coated with the same DBR as described above. All measurements are performed using a dipstick immersed in liquid helium. The sample can be moved in the (x-y) plane using nanopositioners. In addition, the cavity length is adjusted with a z-axis nanopositioner. For transmission, light from a (broadband) LED covering the spectral range of interest is sent through the fiber with the dimple and collected by an aspheric lens. A second LED emitting green light, that overlaps with a transmission window of the DBR mirrors, is used to locate the flake.

For PL measurements, a 532 nm laser is sent through the fiber. This wavelength is within a transmission window outside of the stop band of the DBR. Therefore, PL excitation is efficient and only marginally changing with the cavity length. To extract the PL spectrum, the cavity emission spectrum is measured as a function of cavity length. For each cavity length, the area and the center wavelength of the PL escaping through the cavity mode is measured. Plotting the area against the center wavelength of the cavity mode yields the PL spectrum of the flake.

## CAPACITIVE MODEL FOR THE FERMI ENERGY

By applying a top gate voltage  $V_g$  the electron density in the sample and therefore the Fermi energy  $E_F$  is changed. We denote the smallest  $V_g$  for which the attractive polaron is observed as  $V_g = V_c$  which we interpret as the gate voltage for which we start populating the conduction band ( $E_F > 0$ ).

The capacitance per unit area  $C/A$  between top gate and sample is given by:

$$\frac{C}{A} = \left( \frac{t}{\epsilon\epsilon_0} + \frac{1}{e^2 D(E)} \right)^{-1}, \quad (\text{S28})$$

where  $D(E)$  is the density of states and  $t$ ,  $\epsilon$  are the thickness respectively the permittivity of the hBN flake. The two terms are the geometric respectively quantum capacitance of the sample. For  $E_F > 0$ , the quantum capacitance can be neglected since its effect is much smaller and within the uncertainty of the permittivity of the hBN flake. For  $V_g > V_c$  i.e.  $E_F > 0$  this yields:

$$E_F = \frac{\pi\hbar^2\epsilon\epsilon_0}{tem^*}(V_g - V_c) \approx 0.77 \frac{\text{meV}}{\text{V}}(V_g - V_c), \quad (\text{S29})$$

where  $m^*$  is the effective electron mass of the conduction band.

## SPATIAL DEPENDENCE

One of the principal advantages of the open fiber cavity structure is the ability to adjust the cavity length and to thereby change the nature of coupling. In our setup, the fiber facet and the substrate form a small angle. As a consequence, when the fiber is in close proximity to the facet it touches the substrate. The contact is located at the edge of the fiber which is  $125\ \mu\text{m}$  in diameter. This contact stabilizes the cavity by suppressing the vibrations that would otherwise have lead to line broadening. Furthermore, once the cavity is brought into contact with the substrate, changing the cavity length by changing the piezo voltage of the z-axis nanopositioner seems to be completely reversible. When the cavity length is reduced further to a few micrometers, it is essentially the fiber angle that changes and reduces the cavity length at the dimple which is in the center of the fiber facet.

Additionally, scanning the sample with respect to the fiber mirror allows us to investigate the spatial dependence of the MoSe<sub>2</sub> optical excitations. In order to investigate the latter, the cavity length was enlarged to be sure to eliminate any contact between fiber and substrate. At a cavity length of  $\sim 30\ \mu\text{m}$ , the sample was moved with respect to the fiber mirror with nanopositioner slip-stick steps. The nanopositioner resistive readout was used to get an estimate of the traveled distance. A rough estimate of the cavity position with respect to the flake is obtained using a camera by imaging the flake illuminated with a green LED which is transmitted through a transmission window of the DBR. The spectrum is derived from the cavity linewidth broadening in a cavity length scan using the same technique as for the data shown in Figure 2 of the main text.

Figure S1 shows absorption spectra for different positions of the sample with respect to the cavity. The sample is moved by  $\sim 0.5\ \mu\text{m}$  in between the different measurements. The scan was measured at a gate voltage of  $V_g = -10\ \text{V}$  where we expect to see absorption from both the repulsive and attractive polaron. At  $x = -1.5\ \mu\text{m}$ , the spatial overlap of the cavity mode with the MoSe<sub>2</sub> monolayer is small. As the sample is moved, the overlap and therefore the absorption increases until it reaches a maximum at  $x = 0.0\ \mu\text{m}$ . Moving the sample further up to  $x = 1.5\ \mu\text{m}$  reduces the overlap again. The absorption strength of the attractive polaron as compared to the repulsive polaron does not change significantly depending on the position of the sample which indicates a relatively homogeneous electron density. The large distance over which the absorption decreases is in accordance with the large cavity mode waist of  $1.7\ \mu\text{m}$ .

## CAVITY MODE FITTING

The source for the transmission spectroscopy is a LED centered at  $\sim 760\ \text{nm}$  with a FWHM of  $\sim 20\ \text{nm}$ . For Figure 2a, Figure 3a,b,c and Figure 4a of the main text, the transmitted spectrum is normalized by the LED spectrum. For the derivation of the absorption spectrum of the flake from the transmission spectra shown in Figure 2a of the main text, the normalization with the LED spectrum is not necessary since only the linewidth and the center wavelength of the cavity mode but not the intensity of the transmitted cavity peaks are used to extract the absorption spectrum. In addition to the fundamental cavity mode, higher transverse modes are observed in the transmission spectrum. For fitting the lorentzian peak to the transmitted fundamental cavity mode, only the spectrum within a  $4\ \text{nm}$  wide window was considered in order to exclude distortions from the higher transverse modes.

At the cavity lengths used for weak coupling measurements, more than one fundamental modes are observed within the stop band of the DBR. For the derivation of the energy shift of the cavity due to the resonances of the flake,

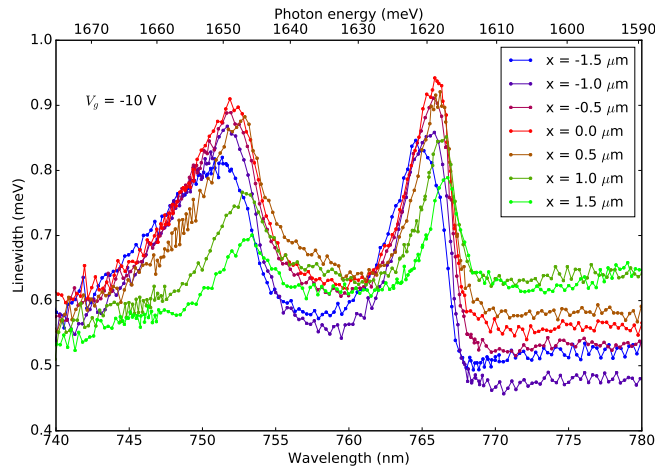


FIG. S1. Spatial dependence of the absorption spectrum.

the cavity length is calculated from the wavelength of the next (lower-energy) fundamental mode. Since the energy of that cavity mode is smaller than any resonances of the MoSe<sub>2</sub> monolayer, its center wavelength serves as a good measure for the cavity length.

We note that for the cavity length of  $9.1 \mu\text{m}$  used to obtain the data depicted in Fig. 2b, the exciton and the cavity are in the strong coupling regime for  $V_g < -10 \text{ V}$ . As a consequence, it is not possible to obtain the imaginary part of the MoSe<sub>2</sub> linear susceptibility by measuring the excess cavity line broadening as we tune the cavity across the exciton (repulsive polaron) resonance. As a remedy, we chose to plot the linewidth of the cavity-like polariton peak for the parameter range corresponding to the dashed box in Fig. 2b. The cavity line broadening we extract in this manner is larger than the actual width of the exciton resonance. It does however, yield the correct exciton resonance frequency. As an alternative, it is possible to extract the actual imaginary part of the MoSe<sub>2</sub> linear susceptibility by fitting the data to a formula that describes the absorption lineshape in the presence of strong coupling [S4] and extract an exciton linewidth of 4.5 meV. The drawback of the latter formula is that it is only accurate if the electronic resonances are Lorentzian; this is satisfied only for  $V_g < -10 \text{ V}$ .

---

[S1] F. Chevy, Physical Review A **74**, 063628 (2006).

[S2] M. M. Parish and J. Levinsen, Physical Review A **87**, 033616 (2013).

[S3] P. J. Zomer, M. H. D. Guimares, J. C. Brant, N. Tombros, and B. J. van Wees, Applied Physics Letters **105**, 013101 (2014), <http://dx.doi.org/10.1063/1.4886096>.

[S4] S. E. Harris, J. E. Field, and A. Imamoglu, Phys. Rev. Lett. **64**, 1107 (1990).